Vibration-assisted coherent excitation energy transfer in a detuned dimer*

Xin Wang(王信)[1,2], Hao Chen(陈浩)[1], Chen-yu Li(李晨宇)[1], and Hong-rong Li(李宏荣)[1,2,†]

[1] School of Science, Xi'an Jiaotong University, Xi'an 710049, China
[2] CEMS, RIKEN, Wako-shi, Saitama 351-0198, Japan

(Received 5 August 2016; revised manuscript received 21 November 2016; published online 18 January 2017)

The important role of high-energy intramolecular vibrational modes for excitation energy transfer in the detuned photosynthetic systems is studied. Based on a basic dimer model which consists of two two-level systems (pigments) coupled to high-energy vibrational modes, we find that the high-energy intramolecular vibrational modes can enhance the energy transfer with new coherent transfer channels being opened when the phonon energy matches the detuning between the two pigments. As a result, the energy can be effectively transferred into the acceptor. The effective Hamiltonian is obtained to reveal the strong coherent energy exchange among the donor, the acceptor, and the high-energy intramolecular. A semi-classical explanation of the phonon-assisted mechanism is also shown.

Keywords: excitation energy transfer, high-energy intramolecular vibrational motion, dynamically resonant coherent transfer

PACS: 71.35.–y, 03.65.Yz, 63.50.–x **DOI:** 10.1088/1674-1056/26/3/037105

1. Introduction

The role of coherent vibrational dynamics on the efficiency of energy transfer in natural and artificial light harvesting systems is currently of central interest.[1] It is known that the functionality of a natural multichromophoric complex depends mainly on the strength and structure of interactions among electronic states and is dramatically affected by the vibrational degrees of freedom associated either with the complex itself or to its environment.[2–5] Among plenty of progress[1,6–9] that has been achieved in experimental and theoretical research on quantum effects in natural light harvesting systems, the positive role of the phonon is increasingly solid.[1] The key mechanism of noise-assisted excitation energy transfer (EET) is one progress that has been identified.[10–13] That is, in the energy-closed EET system, phonon modes perturb the system to suppress the destructive interference and broaden its spectral lines by inducing thermal fluctuations of the on-site energy, thus enhancing excitation transfer. The phonon modes related to noise-assisted EET arise from the low-energy protein vibrations and the solvent, which have a continuous distribution of frequencies that are below or comparable to the thermal energy scale, $k_{\mathrm{B}}T$, and couple to the electronic states weakly comparing with the coupling strength among electronic states. Another kind of phonon modes with high energy and well-localized frequencies are revealed by spectroscopy studies,[14–21] the active participation during the excitation dynamics. These modes originate from intramolecular vibration and couple to the electronic states with strength comparable to that of inter-site electronic interaction.[22–29] The quantum mechanical features of the high-energy vibrational modes are significant even at ambient temperatures[2] and their influence on energy transport in a variety of natural molecular systems is currently of central interest.[17,21,30–32]

This work focuses on the important role of the high-energy vibrational modes for EET in a detuned system of light harvesting, which is similar to that in cryptophyte antennae protein phycoerythrin 545 (PE545).[22,33] Different from the noise-assisted EET situation, the differences of site energy $|\varepsilon_m - \varepsilon_n|$ are very large in comparison to inter-site electronic interaction V_{mn}. In this situation, the excitation energy is highly localized to the donor site and hardly transfers to the next site only with the help of the noise in the surrounding environment. For example, the largest coupling of inter-site electronic interactions in PE545 is $V = 92$ cm^{-1} between the central pigments $\mathrm{PEB}_{50\mathrm{C}}$ and $\mathrm{PEB}_{50\mathrm{D}}$, while their energy difference is about 1040 cm^{-1}.[24] The localized vibrational mode at $\omega = 1111$ cm^{-1} is on near resonance with the transition between $\mathrm{PEB}_{50\mathrm{C}}$ and $\mathrm{PEB}_{50\mathrm{D}}$. The coupling between the vibrational mode and the electronic states of the two sites is $g = 267$ cm^{-1} ($g = \omega\sqrt{s} = 1111$ cm$^{-1} \times \sqrt{0.0578} \approx 267$ cm^{-1}, where ω is the frequency of the intro-molecular vibrational mode, and s is the relative Huang–Rhys factor),[24] which is larger than $V = 92$ cm^{-1}, thus it is possible that the vibrational mode would effectively participate in and even enhance the EET process. Aiming at revealing the fundamental mechanism of a bridge-like role of quasi-resonant vibrations for the excitonic transitions in the above situation, which has

*Project supported by the National Natural Science Foundation of China (Grant No. 11174233).
†Corresponding author. E-mail: hrli@mail.xjtu.edu.cn
© 2017 Chinese Physical Society and IOP Publishing Ltd

also been mentioned by Kolli previously,[24] based on a basic detuned dimer model, we will theoretically study the role that high-energy vibrational modes play in EET.

In our model, the strength of coupling between high-energy vibrational modes and the dimer's electronic state is comparable to that of the dipole–dipole interaction between the donor and the acceptor, while the phonon bath of the environment is weakly coupled to the donor and the acceptor. We will show, by numerical calculation, that high efficiency of EET could be obtained by phonon-assistance in the large-detuned conditions. The effective Hamiltonian will be obtained to reveal a second-order coherent transfer process among the donor, the acceptor, and the high-energy vibrational mode, which enhances the EET by opening up a new transfer channel. The semi-classical explanation of the phonon-assisted mechanism will be shown as well.

The paper is organized as follows. We show our main numerical results of the basic model in Section 2 and the related analysis in Section 3. Investigation of the further model is given in Section 4. Conclusions are finally made in Section 5.

2. Vibration enhancing EET in a dimer

We consider that energy is transferred inside a dimer, which includes pigment 1 (the donor) and pigment 2 (the acceptor), and both pigments are two-level systems with energy separations ε_1 and ε_2, respectively. The Hamiltonian of the dimer is ($\hbar = 1$)

$$H_{\mathrm{D-A}} = \varepsilon_1 \sigma_1^+ \sigma_1^- + \varepsilon_2 \sigma_2^+ \sigma_2^- + V_{12}\left(\sigma_1^+ \sigma_2^- + \sigma_2^+ \sigma_1^-\right), \quad (1)$$

where $\sigma_i^+ = |e_i\rangle\langle g_i|$ and $\sigma_i^- = |g_i\rangle\langle e_i|$ are the transition operators at site i ($i = 1,2$) with energy detuning $\Delta = \varepsilon_1 - \varepsilon_2$, and V_{12} denotes the electronic coupling between sites 1 and 2. The donor is coupled to a vibrational mode with the free Hamiltonian $H_{\mathrm{M}} = \upsilon b^\dagger b$, where υ is the angular eigenfrequency of the vibrational mode, and $b^\dagger$ (b) is the creation (annihilation) operator of the vibrational mode. The Hamiltonian that describes this system is

$$H_1 = H_{\mathrm{D-A}} + H_{\mathrm{M}} + H_{\mathrm{D-M-A}}, \quad (2)$$

where $H_{\mathrm{D-M-A}} = (gb^\dagger + gb)\sigma_1^+\sigma_1^-$, and g is the coupling strength between the vibrational mode and the donor.

We assume that the system is polluted by three incoherent processes: the two pigments dissipate into the environment at rates Γ_1 and Γ_2, respectively; and the acceptor sinks into the RC (sink) at a rate of κ. The vibrational mode decays into the thermal environment at a rate of γ with thermal phonon number $n_{\mathrm{th}} \simeq kT/\hbar\upsilon$, where k is the Boltzmann constant and T is the temperature.

For brevity, hereafter, we set all the parameters to be dimensionless when discussing the numerical results of this theoretical model. As discussed in Ref. [34] (and references therein), the sink rate into RC is much larger than the energy dissipation rate into the thermal environment, and therefore we set $\Gamma_1 = \Gamma_2 = 0.1$ and $\kappa = 3$. Moreover, discrete intramolecular vibrational modes have a very sharp spectrum shape,[35,36] indicating that their quality factor can be very high. In our discussion, we consider the mechanical mode oscillating at frequency $\upsilon = 200$ with decay $\gamma = 0.4$ (i.e., the quality factor is $Q = 500$). All of the processes (the non-unitary) can be described by Lindblad terms $D[A,\Omega]\hat{\rho} = \Omega(A\hat{\rho}A^+ - \frac{1}{2}A^+A\hat{\rho} - \frac{1}{2}\hat{\rho}A^+A)$. Thus, we can write the master equation of the whole system as

$$\begin{aligned}\frac{\mathrm{d}\hat{\rho}(t)}{\mathrm{d}t} &= -\mathrm{i}\,[H_{1\mathrm{I}}, \hat{\rho}(t)] + D[\sigma_1^-, \Gamma_1]\hat{\rho}(t) \\ &\quad + D[\sigma_2^-, \Gamma_2]\hat{\rho}(t) + D[\sigma_2^-, \kappa]\hat{\rho}(t) \\ &\quad + n_{\mathrm{th}} D[b^+, \gamma]\hat{\rho}(t) + (n_{\mathrm{th}}+1) D[b, \gamma]\hat{\rho}(t), \quad (3)\end{aligned}$$

where $\hat{\rho}$ is the density matrix operator for the system, and $H_{1\mathrm{I}}$ is the interaction Hamiltonian

$$\begin{aligned}H_{1\mathrm{I}} &= \Delta\sigma_1^+\sigma_1^- + \upsilon b^\dagger b + V_{12}\left(\sigma_1^+\sigma_2^- + \sigma_2^+\sigma_1^-\right) \\ &\quad + (gb^\dagger + gb)\sigma_1^+\sigma_1^-, \quad (4)\end{aligned}$$

which is obtained by performing a unitary transformation $U_0(t) = \exp(\mathrm{i}H_0 t)$ to H_1 with $H_0 = \varepsilon_2(\sigma_1^+\sigma_1^- + \sigma_2^+\sigma_2^-)$.

We define two probabilities $P_i(t) = \mathrm{Tr}[|e_i\rangle\langle e_i|\hat{\rho}(t)]$ ($i = 1,2$). If the dissipation rate of the acceptor into the sink is defined as $R(t) = \kappa\langle e_2|\hat{\rho}(t)|e_2\rangle$, the energy transfer efficiency at a fixed time t will be calculated by $\eta(t) = \int_0^t R(t')\mathrm{d}t'$.[37] We assume that the two pigments are initially in $|e_1, g_2\rangle$, and our numerical simulation is based on the single excitation subspace.[38] To approach the actual environmental conditions, in all of the following numerical calculations, we assume that the vibrational mode has reached the thermal equilibrium state and the associated density matrix is

$$\mu(0) = \sum_n \frac{n_{\mathrm{th}}^n}{(n_{\mathrm{th}}+1)^{n+1}} |n\rangle\langle n|,$$

where $|n\rangle$ represents the Fock state of the vibrational mode with phonon number n. Thus, the initial density matrix for the whole system can be expressed as $\hat{\rho}(0) = |e_1, g_2\rangle\langle e_1, g_2| \otimes \mu(0)$. We then perform numerical simulations based on master equation (3).

To capture the fundamental mechanism of high-energy-phonon-assisted EET, we focus on the situation that only the donor is coupled to the vibrational mode in this section. The time-dependent probabilities and efficiency are plotted in Fig. 1, where the parameters are chosen according to the real PE545 system (not the exact values, but the ratio of those parameters mentioned in the introduction). Comparing Figs. 1(a) and 1(b), we find that the evolutions of the system are significantly different with and without the donor coupling to the

vibrational mode. When the donor is decoupled from the vibrational mode (Fig. 1(b)), $P_2(t) \simeq 0$, which means that the acceptor is hardly excited and the efficiency is very low because of large detuning. In this case, most of the energy leaks out from the donor through dissipative processes and cannot be transferred to the acceptor. However, when the vibrational mode takes part (Fig. 1(a)), the situation is totally different: the acceptor has a high probability of being excited, and the efficiency can reach above 80%.

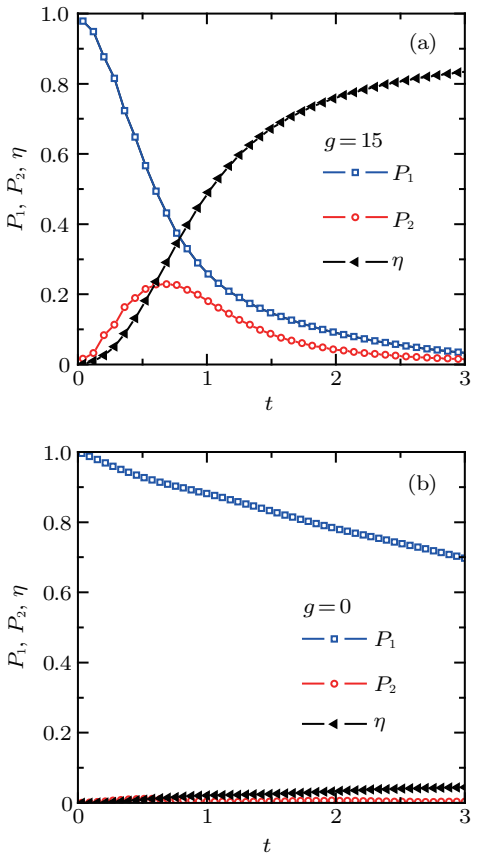


Fig. 1. (color online) Numerical results of the change in probabilities $P_1(t)$ and $P_2(t)$, and the efficiency $\eta(t)$ with time for $\Delta = \upsilon = 200, V_{12} = 15, \Gamma_1 = \Gamma_2 = 0.1$, $\kappa = 3$, $\gamma = 0.4$, and $n_{\rm th} = 1$.

The numerical results with different initial thermal states are shown in Fig. 2. It can be found that, even the thermal phonon number is extremely low with $n_{\rm th} = 0.1$, the energy transfer efficiency is also apparently increased. Compared with the case of $n_{\rm th} = 0.1$, both the transfer efficiency $\eta(t)$ and the probability $P_2(t)$ are higher in the case of $n_{\rm th} = 2$, and the system reaches its steady state faster. When the average phonon number $n_{\rm th}$ of the initial state increases, the effective coupling strength increases. As a result, the energy can be transferred to the acceptor with a higher efficiency in a shorter period of time. Figure 2(b) shows that the efficiency $\eta(t)$ increases with $n_{\rm th}$ under different coupling strength g when the system reaches its steady state. The effect of increasing $n_{\rm th}$ is apparent when the coupling is relatively weak ($g = 5$), although the effect is not so obvious when the coupling is much stronger (e.g., $g = 15$).

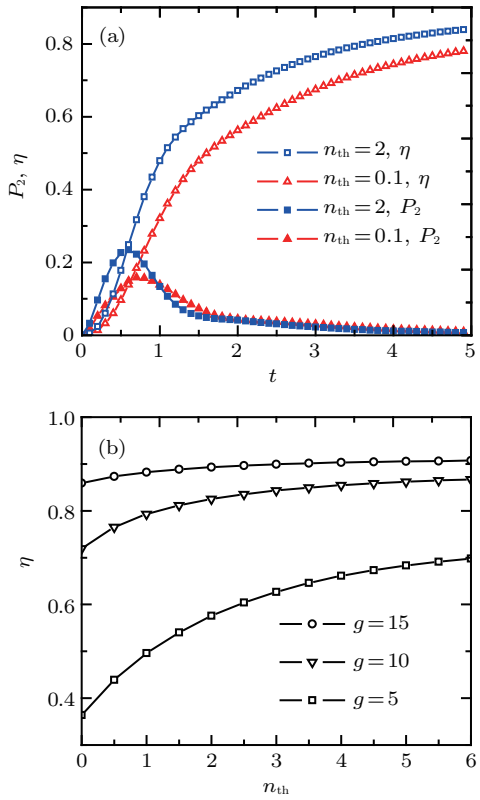


Fig. 2. (color online) (a) Evolution of $\eta(t)$ and $P_2(t)$ with $n_{\rm th} = 0.1$ and $n_{\rm th} = 2$ and the same parameters as those in Fig. 1(a). (b) η as a function of $n_{\rm th}$ for coupling strengths $g = 5$, $g = 10$, and $g = 15$ when $t = 10$ and the system has reached its steady state.

Here we should stress that, in this theoretical model, the efficiency of EET will benefit from higher environment temperature. However, in realistic cases, the situation might be much more complex. For example, at too high or too low temperature, the bioactive light-harvesting molecular might not behave so well as at a proper temperature. There will be a trade-off relation when increasing the temperature of the system. The energy transfer efficiency is not just a simple thermal monotone, and the results above only work well under special environment conditions.

3. Analysis

From the above section, we find that a high-energy-intramolecular vibrational mode can enhance the EET in the detuned dimer system. The physical mechanism of such enhancement, as well as a semi-classical explanation, are studied in this section.

To reveal the physical mechanism of such enhancement, we firstly derive the effective Hamiltonian of the hybrid system containing the donor, the acceptor, and the vibrational mode. Starting from Eq. (4) and assuming that the coupling is weak (i.e., $\upsilon \gg \{g, V_{12}\}$), we obtain the effective Hamiltonian under the condition $\Delta = \upsilon$ (see the detail in Appendix

A):

$$H_{1,\mathrm{eff}} = \left(\frac{V_{12}^2}{\Delta} - \frac{g^2}{\Delta}\right)|e_1\rangle\langle e_1| - \frac{V_{12}^2}{\Delta}|e_2\rangle\langle e_2| - \frac{V_{12}g}{\Delta}(b\sigma_1^+\sigma_2^- + b^\dagger\sigma_1^-\sigma_2^+). \quad (5)$$

From Eq. (5), we find that the last term in the effective Hamiltonian describes a coherent transfer among the donor, the acceptor, and the vibrational mode with rate $V_{12}g/\Delta$. Moreover, because the effective spin–boson coupling strength is proportional to $\sqrt{n+1}$,[39] when the initial phonon number n is very large, i.e.,

$$\sqrt{n+1}\frac{V_{12}g}{\Delta} \gg \left\{\frac{V_{12}^2}{\Delta} - \frac{g^2}{\Delta}, \frac{V_{12}^2}{\Delta}\right\},$$

we can ignore the energy shift terms in $H_{1,\mathrm{eff}}$ and obtain the simpler form of the effective Hamiltonian

$$H'_{1,\mathrm{eff}} = -\frac{V_{12}g}{\Delta}(b\sigma_1^+\sigma_2^- + b^\dagger\sigma_1^-\sigma_2^+). \quad (6)$$

The new form of the effective Hamiltonian $H'_{1,\mathrm{eff}}$ includes only coherent transfer terms inside the system. To understand this process more clearly based on the effective Hamiltonian, we show the energy level configuration in Fig. 3. We find that the energy can be transferred from the donor to the acceptor (the solid blue lines) with the phonon number increasing from n to $n+1$. That is, the detuned energy Δ (the excess energy) between the donor and the acceptor leaks into the vibrational mode during the transition process.

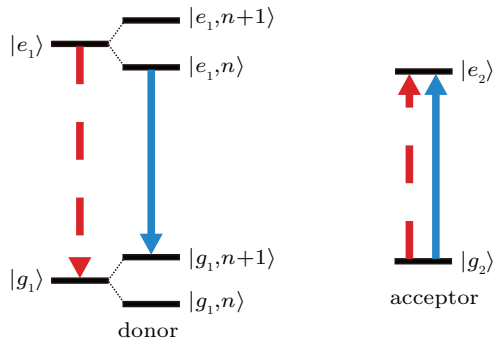


Fig. 3. (color online) Configurations of the energy levels and transitions are shown when the donor is coupled to a vibrational mode. The red (dashed) arrow lines represent the original detuned energy transfer process, which hardly succeed due to the mismatched energy levels. The blue (solid) arrow lines show the phonon-assisted energy transfer process.

For the incoherent initial thermal state

$$\mu(0) = \sum_n \frac{n_{\mathrm{th}}^n}{(n_{\mathrm{th}}+1)^{n+1}}|n\rangle\langle n|,$$

we can first obtain $P_{2,n}(t) = \mathrm{Tr}[|e_2\rangle\langle e_2|\hat{\rho}_n(t)]$ by individually solving master equation (3) with the initial state $\hat{\rho}_n(0) = |e_1,g_2,n\rangle\langle e_1,g_2,n|$ $(n = 1,2,3,\ldots)$ for different n. Because $\mu(0)$ is only an incoherent mixed state with different Fock states, there is no coherence between $\rho_n(t)$, and we then obtain the weighted average

$$P_2(t) = \sum_n \frac{n_{\mathrm{th}}^n}{(n_{\mathrm{th}}+1)^{n+1}}P_{2,n}(t).$$

For each n, when the vibrational mode is coupled with the EET system, there will be coherent transfer between states $|e_1,g_2,n\rangle$ and $|g_1,e_2,n+1\rangle$. It means that the energy can be transferred to the acceptor, and as a result, the phonon number of the vibrational mode increases from n to $n+1$, as shown in Fig. 3. Direct energy transfer from the donor to the acceptor without assistance of the vibrational mode is not an energy conservation process. However, the transfer between states $|e_1,g_2,n\rangle$ and $|g_1,e_2,n+1\rangle$ with the assistance of the vibrational mode satisfies energy conservation ($\varepsilon_1 = \varepsilon_2 + \upsilon$). Thus, it has a high probability of occurring.

To show the validations of the effective Hamiltonian, we compare the results determined by $H_{1\mathrm{I}}$, $H_{1,\mathrm{eff}}$, and $H_{1,\mathrm{eff}'}$ by plotting the probabilities $P_2(t)$ in Figs. 4(a)–4(c), where we assume that the initial state of the system is $|e_1,g_2,n\rangle$ and do not consider decoherent effects, and $|n\rangle$ represents the Fock state of the vibrational mode with phonon number n.

In Fig. 4(a), excitation of the acceptor occurs with a very low probability when there is no assistance of the vibrational mode. When the vibrational mode takes effect, as shown in Fig. 4(b), coherent transfer in this hybrid system emerges and the acceptor has a high probability of being excited. Since the detuning energy will leak into the vibration mode, rather than absorbing a phonon from the mechanical oscillator, our model also works well when the initial phonon number is zero or extremely low (see Figs. 2(a) and 4(b)). The consistency between $H_{1,\mathrm{eff}}$ and $H_{1\mathrm{I}}$ under the weak coupling approximation is determined by comparing Figs. 4(b) and 4(c). In Fig. 4(b), as the coupling strength g is much weaker than the detuning Δ, the approximation for obtaining the effective Hamiltonian $H_{1,\mathrm{eff}}$ from $H_{1\mathrm{I}}$ is valid. However, when the coupling strength increases, differences in the figures can be observed, as shown in Fig. 4(c), and the dynamics of probabilities $P_2(t)$ determined by $H_{1,\mathrm{eff}}$ does not match well with that determined by $H_{1\mathrm{I}}$. As shown in Fig. 4(d), when $n = 6$, the effects of energy shift terms in $H_{1,\mathrm{eff}}$ are suppressed, the evolutions described by $H_{1,\mathrm{eff}'}$ and $H_{1\mathrm{I}}$ match well, and $P_2(t)$ can reach nearly 1. We should mention here that increasing the phonon number at a certain range will enhance $P_2(t)$.

The mechanism of the coherent energy transfer of our system can also be described semi-classically. The vibration–donor coupling term $H_{\mathrm{D-M}} = g(b^\dagger + b)\sigma_1^+\sigma_1^-$ can be rewritten as $H_{\mathrm{D-M}} = F(t)x$, where $F(t) = gP_1(t)/a_0$, $x = a_0(b^\dagger + b)$, and a_0 is the zero-point fluctuation of position amplitude for the vibrational mode.[40] The new form of $H_{\mathrm{D-M}}$ indicates that injection of an exciton of the donor creates an instantaneous force on the vibrational mode.[35] The Rabi oscillation between the donor and the acceptor can be expressed as

$\Omega_r = \sqrt{\Delta^2 + 4V_{12}^2}$, which will produce a time-oscillating force on the vibration mode.

If the interaction between the donor and the acceptor is of large detuning, the Rabi oscillation with small amplitude for $P_1(t)$ at the central frequency around $\Omega_r \simeq \Delta$ must exist.[39] By setting other parameters the same as those in Fig. 1, the distribution of the amplitude $A_1(\omega)$ (ω is the angular frequency at the frequency domain) of the Fourier transform of $P_1(t)$ is shown in Fig. 5, in which there is a peak around the eigenfrequency of the vibrational mode, i.e., $\omega \simeq 200$. Moreover, in Fig. 5(b), we show that the efficiency η changes with the frequency of the vibration mode. It can be found that, at $\nu = \Omega_r \simeq 202$ (i.e., the force $F(t)$ is on resonance with the vibration mode), the efficiency η reaches its maximum. With the detuning increasing, η will decrease rapidly. It is similar to the following scene: when someone pushes a swing on its intrinsic frequency, although it is only a very weak force, the swing will oscillate with high amplitude after a relatively long time.[36,41] For this hybrid system, the excess energy $\varepsilon_1 - \varepsilon_2 = \Delta$ will leak into the vibrational mode resonantly.

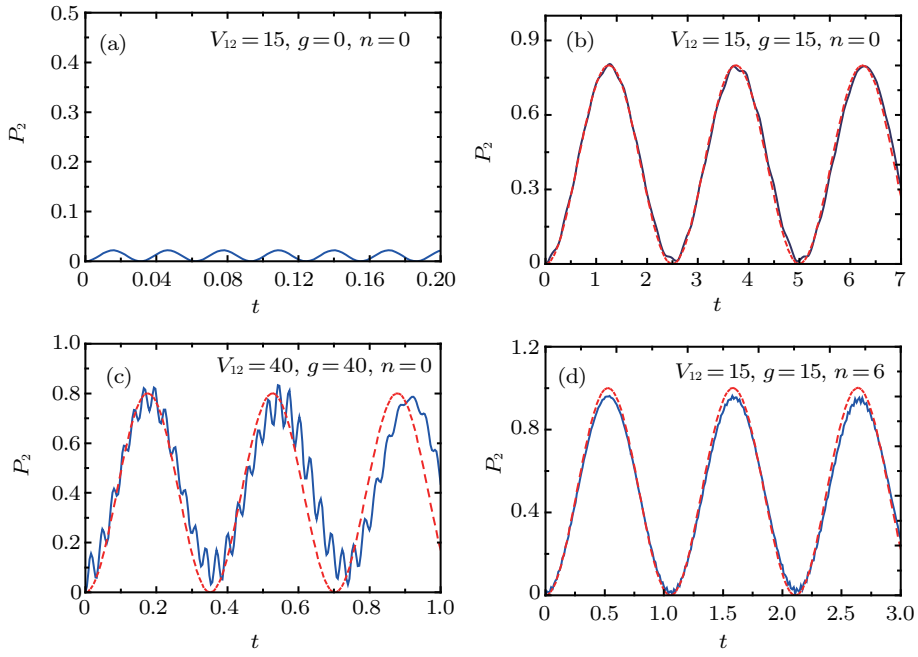


Fig. 4. (color online) Probabilities $P_2(t)$ versus time for different cases determined by Hamiltonian H_{1I} (blue solid lines in panels (a)–(d)), $H_{1,\text{eff}}$ (red dashed line in panels (b) and (c)), and $H'_{1,\text{eff}}$ (red dashed line in panel (d)). Here, we set $\Delta = \upsilon = 200$.

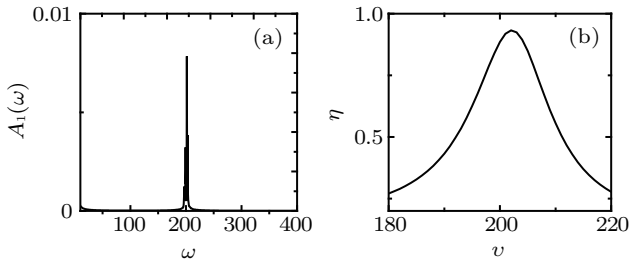


Fig. 5. (a) Amplitude $A_1(\omega)$ of the Fourier transform of $P_1(t)$ at the frequency domain. (b) The EET efficiency η changes with the frequency of the mechanical oscillator. The parameters used are the same as those in Fig. 1(a).

Lastly, we want to discuss the case that the dipole coupling between the donor and the acceptor is comparable (or stronger) to the detuning between the donor and the acceptor. In this case, the large detuning assumption adopted to derive the effective Hamiltonian (in the Appendix) is not valid again. Therefore, we cannot use $H_{1,\text{eff}}$ to describe the evolution of the systems. However, we can still use the semiclassical analysis to confirm what frequency of the vibration mode should be adopted to increase the EET efficiency. Considering that the coupling strength is much stronger than the detuning, i.e., $V_{12} = 2\Delta = 400$, the Rabi oscillation frequency is $\Omega_r = \sqrt{\Delta^2 + 4V_{12}^2} = 824$. Here we should shift the vibration mode to $\nu = \Omega_r$, and plot the evolution for the system with and without coupling to the mechanical mode, which is shown in Fig. 6. It can be found that, for the case that the system couples with the vibrations, the energy transfer needs less time and is of higher efficiency than that when the donor decouples from the vibration mode, indicating that our model still works even when the coupling is very strong. The mechanical mode can also assist the energy transfer under the condition that its frequency is resonant with the donor-acceptor Rabi oscillation. Moreover, the evolutions of P_2 in the two cases are totally different: when the vibration mode takes effect, P_2 does not oscillate rapidly and maintains a relatively high value due to the resonance with the mechanical mode. However, the effect is not so apparent as it is in the weak coupling case (Figs. 1(a) and 1(b)). In conclusion, our model can increase the EET efficiency in both weak and strong dipole coupling cases, and behaves better when the coupling is much weaker than the detuning.

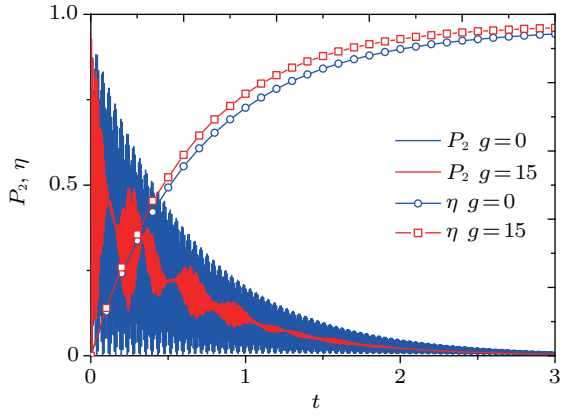


Fig. 6. (color online) The case when the coupling strength between the donor and the acceptor is stronger than the detuning, i.e., $V_{12} = 2\Delta = 400$. To induce a resonant drive strength for the mechanical mode, we set $\Omega_r = \sqrt{\Delta^2 + 4V_{12}^2} = 824$. We plot the cases with and without assistance of the vibration mode (i.e., $g = 15$ and $g = 0$). It is clearly shown that, even in the strong coupling case, our model can still increase the efficiency of EET to some extent. The other parameters used here are the same as those in Fig. 1(a).

4. Further investigation

In the above two sections, we have investigated the numerical results, the physical mechanism, and the semiclassical explanation of the EET in a detuned dimer system when the donor is coupled to a vibrational mode. Based on the above investigation, which has revealed the foundation of the vibration-enhanced EET, further results will be obtained in the more complex and realistic models in this section.

The first more complex model is that both the donor and acceptor are coupled to an identical vibrational mode. The Hamiltonian describing the system is

$$H_2 = H_{\mathrm{D-A}} + H_{\mathrm{M}} + H'_{\mathrm{D-M-A}}, \tag{7}$$

where $H'_{\mathrm{D-M-A}} = (g_1 b^\dagger + g_1^* b)\sigma_1^+\sigma_1^- + (g_2 b^\dagger + g_2^* b)\sigma_2^+\sigma_2^-$, and g_1 and g_2 are the coupling strengths of the vibrational mode for the donor and the acceptor, respectively. Without loss of generality, we assume that g_1 is real and $g_2 = |g_2|\mathrm{e}^{\mathrm{i}\theta}$, where θ is the relative phase of g_1 and g_2. It is obvious that the relative phase plays roles on EET in the system. $P_2(t)$ and $\eta(t)$ are plotted in Fig. 7 for this model.

In Fig. 7(a), the three cases with $\theta = 0$, $\theta = \pi/3$, and $\theta = \pi$ are shown. The relative coupling phase of g_1 and g_2 significantly affects the dynamics of the system. Compared with the case of $\theta = \pi/3$, for the case of $\theta = \pi$, the efficiency $\eta(t)$ increases faster and the peak of $P_2(t)$ is much higher and comes earlier. Correspondingly, the steady η of the case with $\theta = \pi$ is higher than that of the case with $\theta = \pi/3$. In contrast, the situation with $\theta = 0$ is quite similar to the case with no assistance of the vibrational mode. The dependency of steady η on θ is shown in Fig. 7(b). The steady η greatly changes depending on the relative coupling phase.

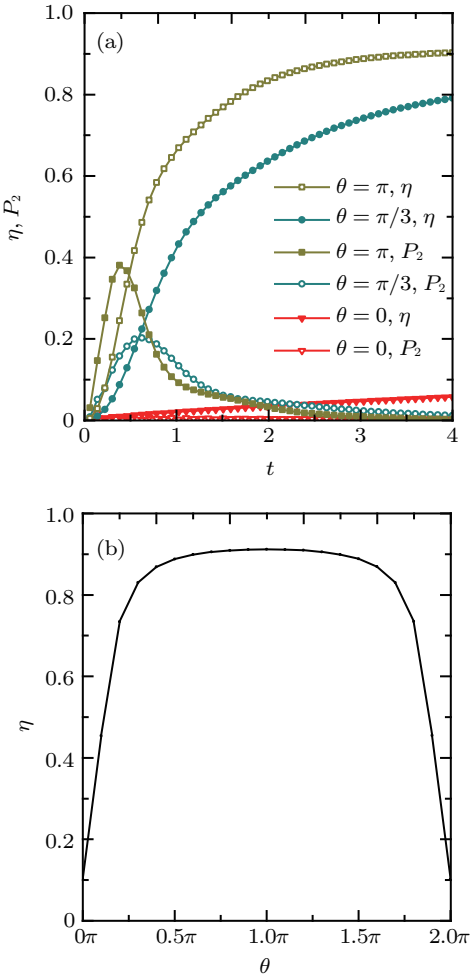


Fig. 7. (color online) (a) $\eta(t)$ and $P_2(t)$ versus time for $\theta = 0, \theta = \pi/3$, and $\theta = \pi$, and (b) η as a function of θ when $t = 10$. The parameters are the same as those in Fig. 1(a) except $g_1 = |g_2| = 15$.

For this model, we obtain an effective Hamiltonian $H_{2,\mathrm{eff}}$ by assuming that $\Delta = \upsilon \gg \{g_1, g_2, V_{12}\}$,

$$\begin{aligned} H_{2,\mathrm{eff}} = & \left(\frac{V_{12}^2}{\Delta} - \frac{g_1^2}{\Delta}\right)|e_1\rangle\langle e_1| - \left(\frac{V_{12}^2}{\Delta} + \frac{|g_2|^2}{\Delta}\right)|e_2\rangle\langle e_2| \\ & - \frac{2g_1|g_2|}{\Delta}\cos\theta\,|e_1\rangle\langle e_1| \otimes |e_2\rangle\langle e_2| \\ & + \frac{V_{12}(g_2^* - g_1)}{\Delta} b\sigma_1^+\sigma_2^- \\ & + \frac{V_{12}(g_2 - g_1)}{\Delta} b^\dagger\sigma_1^-\sigma_2^+. \end{aligned} \tag{8}$$

The first three terms in $H_{2,\mathrm{eff}}$ are the energy shifts caused by the coupling among the three sub-systems. The last two terms in $H_{2,\mathrm{eff}}$ represent coherent transfer with rate $V_{12}(g_2 - g_1)/\Delta$, which shows that the difference of the two coupling strengths has a significant effect on the coherent transfer process. As shown in Fig. 8, there are two transition channels interfering with each other through coupling with the identical vibrational mode; excess energy Δ leaks into the vibrational mode via coupling with the donor or the acceptor at rates of $-V_{12}g_1/\Delta$ (red curve) or $V_{12}g_2/\Delta$ (blue curve), respectively. The coupling phase θ will determine whether the quantum interference between the two channels is destructive or constructive.

Because $V_{12}(g_2 e^{i\theta} - g_1)/\Delta = 0$ when $\theta = 0$ and $|g_2| = g_1$, the energy can hardly be transferred from the donor to the acceptor under these conditions. However, when $\theta = \pi$, the quantum interference between the two channels becomes constructive and the coherent transfer rate is $2V_{12}g_1/\Delta$, which means that there is a high probability of energy transferring into the acceptor.

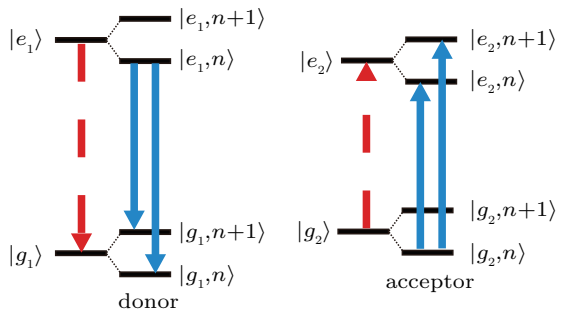


Fig. 8. (color online) Configurations of the energy levels and transitions when both donor and acceptor are coupled to an identical vibrational mode. The red (dashed) arrow lines represent the original detuned energy transfer process, which hardly succeeds due to the mismatched energy levels. The blue (solid) arrow lines show the phonon-assisted energy transfer process.

We also give the semiclassical explanation of the second case from $H_{\mathrm{D-M-A}}$ when $\theta = 0$ and $\theta = \pi$. The Hamiltonian can be rewritten as $H_{\mathrm{D-M-A}} = (F_1(t) + F_2(t))x$, where $F_i(t) = g_i P_i(t)/a_0$ $(i = 1, 2)$. Different from that in the basic model in Section 2, these two forces $F_1(t)$ and $F_2(t)$ are induced by the donor and the acceptor, respectively. In Fig. 9, we plot the amplitude image $A_i(\omega)$ and phase image $\Theta_i(\omega)$ of the Fourier transform of $P_i(t)$ $(i = 1, 2)$ and calculate the phase difference $\Theta(\omega) = \Theta_1(\omega) - \Theta_2(\omega)$ in the frequency domain, where the parameters used are the same as those in Fig. 1(a) except $g_1 = |g_2| = 15$.

In Figs. 9(a) and 9(b), the peaks of $A_1(\omega)$ and $A_2(\omega)$ are located at $\omega = \upsilon = 200$ irrespective of whether $\theta = 0$ or $\theta = \pi$. However, the phase differences $\Theta(\omega)$ always equal π (shown in Figs. 9(c) and 9(d)), which means that $P_1(t)$ and $P_2(t)$ always have opposite signs. When $\theta = 0$, the forces induced by the donor and the acceptor are opposite. As a result, the energy can hardly leak into the vibrational mode. For the case of $\theta = \pi$, the total relative phase of $F_1(t)$ and $F_2(t)$ equals 0, which indicates that the directions of the forces induced by the donor and the acceptor are the same, and thus the excess energy can effectively leak into the vibrational mode.

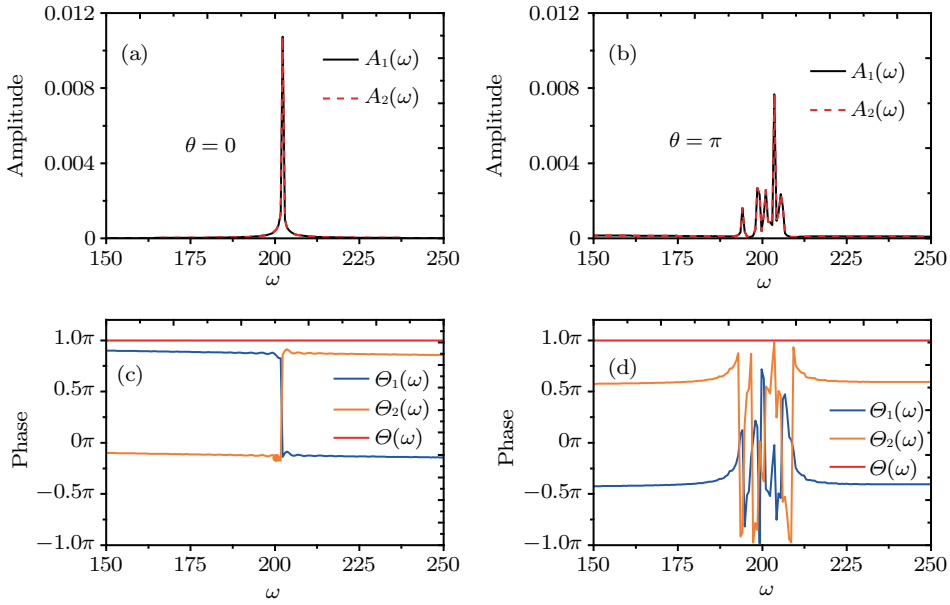


Fig. 9. (color online) (a) and (b) Amplitude images $A_1(\omega)$ (black line) and $A_2(\omega)$ (red dashed line) when $\theta = 0$ and $\theta = \pi$ respectively. (c) and (d) Phase image $\Theta_1(\omega)$ (blue line), $\Theta_2(\omega)$ (yellow line), and $\Theta(\omega)$ (red line) when $\theta = 0$ and $\theta = \pi$ respectively.

We now discuss the second more complex model, where the donor and the acceptor are coupled with different vibrational modes. The Hamiltonian can be expressed as

$$H_3 = H_{\mathrm{D-A}} + H'_{\mathrm{M}} + H_{\mathrm{D-M_{12}-A}}, \tag{9}$$

where $H'_{\mathrm{M}} = \upsilon_1 b_1^\dagger b_1 + \upsilon_2 b_2^\dagger b_2$, $H_{\mathrm{D-M_{12}-A}} = (g_1 b_1^\dagger + g_1^* b_1)\sigma_1^+\sigma_1^- + (g_2 b_2^\dagger + g_2^* b_2)\sigma_2^+\sigma_2^-$, υ_1 and υ_2 are the angular eigenfrequencies of mode 1 and mode 2, respectively; $b_i^\dagger$ (b_i) is the creation (annihilation) operator of vibrational mode i, and g_i represents the coupling strength of pigment i to the associated vibrational modes. We assume that g_1 is real and $g_2 = |g_2| e^{i\theta}$, where θ is the relative coupling phase. Under $\Delta = \upsilon_1 = \upsilon_2 \gg \{g_1, g_2, V_{12}\}$, we obtain the effective Hamiltonian for H_3 as

$$\begin{aligned} H_{3,\mathrm{eff}} = & \left(\frac{V_{12}^2}{\Delta} - \frac{g_1^2}{\Delta}\right)|e_1\rangle\langle e_1| - \left(\frac{V_{12}^2}{\Delta} + \frac{|g_2|^2}{\Delta}\right)|e_2\rangle\langle e_2| \\ & - \frac{V_{12}g_1}{\Delta}(b_1\sigma_1^+\sigma_2^- + b_1^\dagger\sigma_1^-\sigma_2^+) \\ & + \frac{V_{12}}{\Delta}(g_2^* b_2\sigma_1^+\sigma_2^- + g b_2^\dagger\sigma_1^-\sigma_2^+). \end{aligned} \tag{10}$$

There are also two transition channels for energy transfer from the donor to the acceptor: energy can be transferred from the donor to the acceptor with creation of a phonon in mode 1 (being coupled with pigment 1) or in mode 2 (being coupled to pigment 2). That is, the excess energy Δ leaks into vibrational mode 1 or mode 2, which is similar to case 2. However, these two channels are independent because the two modes are independent. Thus, there is no coherent cancellation and the relative coupling phase θ does not affect the evolution of the whole system, which is shown by the numerical results in Fig. 10 with $\theta = 0$ and $\theta = \pi$. When the initial state is $\hat{\rho}(0) = |e_1, g_2\rangle\langle e_1, g_2| \otimes \mu_1(0) \otimes \mu_2(0)$, where $\mu_1(0)$ and $\mu_2(0)$ are the thermal states for vibrational modes 1 and 2 with $n_{\rm th} = 1$, the evolutions of $P_2(t)$ and $\eta(t)$ for $\theta = 0$ and $\theta = \pi$ coincide (blue lines marked with triangles in Fig. 10). Moreover, because both channels take effect, the efficiency $\eta(t)$ increases more quickly and the steady value is slightly higher than those of the case with $g_2 = 0$ (red lines marked with squares in Fig. 10), which corresponds to the model in which only the donor is coupled to the vibrational mode.

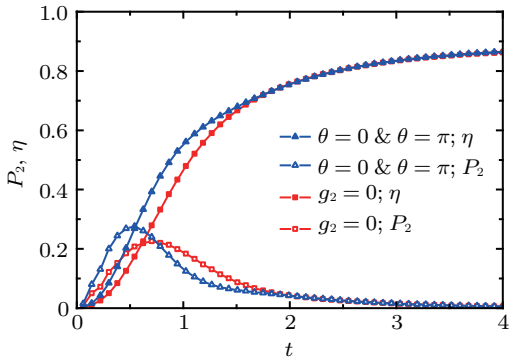


Fig. 10. (color online) Evolution of the second more complex model. The parameters used here are the same as those in Fig. 1(a) except $g_1 = |g_2| = 15$ (blue curve) or $g_1 = 15$ and $g_2 = 0$ (red curve).

5. Conclusion

In summary, we have investigated the energy transfer process between two pigments (simulated by two two-level detuned systems) assisted by the vibrational modes. By analyzing the effective Hamiltonian of the system, we found that there are second-order coherent transfer channels in these hybrid systems. The excess energy (detuning between two two-level systems) can leak into the vibrational modes via these channels, and thus both coherence and EET efficiency can be significantly improved. By assuming that the vibrational modes are initially in incoherent thermal states, we found that the EET efficiency is higher in a relatively high temperature environment. We also found that the quantum interference between two transfer channels plays an important role in the evolution of the system and greatly affects the final EET efficiency. Our results may open up experimental possibilities to investigate and explore detuned coherent transfer phenomena in artificial and natural excitation energy transfer systems.

Appendix A: Steps for obtaining the effective Hamiltonian $H_{1,\rm eff}$

We start from $H_{1\rm I}$. Performing a unitary transformation $U_{\rm A1}(t) = \exp({\rm i}H_{\rm A1}t)$ to $H_{1\rm I}$ with $H_{\rm A1} = \Delta\sigma_1^+\sigma_1^- + \upsilon b^\dagger b$, we then obtain

$$H_{\rm AI}(t) = V_{12}\left(\sigma_1^+\sigma_2^-\,{\rm e}^{{\rm i}\Delta t} + \sigma_2^+\sigma_1^-\,{\rm e}^{-{\rm i}\Delta t}\right) + g(b^\dagger\,{\rm e}^{{\rm i}\upsilon t} + b\,{\rm e}^{-{\rm i}\upsilon t})\sigma_1^+\sigma_1^-. \tag{A1}$$

By assuming $\Delta = \upsilon$, $H_{\rm AI}(t)$ can be rewritten as

$$H_{\rm AI}(t) = B\,{\rm e}^{{\rm i}\Delta t} + B^\dagger\,{\rm e}^{-{\rm i}\Delta t}, \tag{A2}$$

where $B = (V_{12}\sigma_1^+\sigma_2^- + gb^\dagger\sigma_1^+\sigma_1^-)$.

Assuming that the detuning Δ is much larger than the coupling strength $\{g, V_{12}\}$, and focusing on the evolution over a period much longer than the period of any of the oscillations of the system, we can express the effective Hamiltonian as[42]

$$\begin{aligned} H_{\rm A1,eff} &= \frac{1}{\Delta}(BB^\dagger - B^\dagger B) \\ &= \frac{V_{12}^2}{\Delta}(|e_1g_2\rangle\langle e_1g_2| - |e_2g_1\rangle\langle e_2g_1|) \\ &\quad - \frac{g^2}{\Delta}|e_1\rangle\langle e_1| - \frac{V_{12}g}{\Delta}(b\sigma_1^+\sigma_2^- + \sigma_1^-\sigma_2^+). \end{aligned} \tag{A3}$$

The first term in $H_{\rm A1,eff}$ represents the energy shift caused by the coupling between the donor and the acceptor, and the second term represents the energy shift caused by the interaction between the vibrational mode and the donor. Using the relationship $|e_i\rangle\langle e_i| + |g_i\rangle\langle g_i| = I$ $(i = 1, 2)$, we can then rewrite $H_{\rm A1,eff}$ as

$$\begin{aligned} H_{\rm A1,eff} &= \left(\frac{V_{12}^2}{\Delta} - \frac{g^2}{\Delta}\right)|e_1\rangle\langle e_1| - \frac{V_{12}^2}{\Delta}|e_2\rangle\langle e_2| \\ &\quad - \frac{V_{12}g}{\Delta}(b\sigma_1^+\sigma_2^- + b^\dagger\sigma_1^-\sigma_2^+). \end{aligned} \tag{A4}$$

References

[1] Levi F, Mostarda S, Rao F and Mintert F 2015 *Rep. Prog. Phys* **78** 082001
[2] Renger T, May V and Kühn O 2001 *Phys. Rep.* **343** 137
[3] Roden J, Schulz G, Eisfeld A and Briggs J 2009 *J. Chem. Phys.* **131** 044909
[4] Renger T, Madjet M E, Knorr A and Müh F 2011 *J. Plant Physiol.* **168** 1497
[5] Hossein-Nejad H, Olaya-Castro A and Scholes G D 2012 *J. Chem. Phys.* **136** 024112
[6] Ishizaki A, Calhoun T R, Schlau-Cohen G S and Fleming G R 2010 *Phys. Chem. Chem. Phys.* **12** 7319
[7] Scholes G D, Fleming G R, Olaya-Castro A and van Grondelle R 2011 *Nat. Chem.* **3** 763
[8] Olaya-Castro A and Scholes G D 2011 *Int. Rev. Phys. Chem.* **30** 49
[9] Collini E 2013 *Chem. Soc. Rev.* **42** 4932
[10] Plenio M B and Huelga S F 2008 *New J. Phys.* **10** 113019
[11] Chin A W, Datta A, Caruso F, Huelga S F and Plenio M B 2010 *New J. Phys.* **12** 065002
[12] Caruso F, Chin A W, Datta A, Huelga S F and Plenio M B 2013 *J. Chem. Phys.* **131** 105106

[13] Huelga S F and Plenio M B 2013 *Contemp. Phys.* **54** 181

[14] Wendling M, Pullerits T, Przyjalgowski M A, Vulto S I E, Aartsma T J, Van Grondelle R and Van Amerongen H 2000 *J. Phys. Chem. B* **104** 5825

[15] Rätsep M, Pieper J, Irrgang K D and Freiberg A 2008 *J. Phys. Chem. B* **112** 110

[16] Womick J M and Moran A M 2009 *J. Phys. Chem. B* **113** 15747

[17] Womick J M and Moran A M 2011 *J. Phys. Chem. B* **115** 1347

[18] Jankowiak R, Reppert M, Zazubovich V, Pieper J and Reinot T 2011 *Chem. Rev.* **111** 4546

[19] West B A, Womick J M, McNeil L E, Tan K J and Moran A M 2011 *J. Phys. Chem. B* **115** 5157

[20] Eisenmayer T J, de Groot H J M, van de Wetering E, Neugebauer J and Buda F 2012 *J. Phys. Chem. Lett.* **3** 694

[21] Richards G H, Wilk K E, Curmi P M G, Quiney H M and Davis J A 2012 *J. Phys. B* **45** 154015

[22] Doust A B, Marai C N J, Harrop S J, Wilk K E, Curmi P M G and Scholes G D 2004 *J. Mol. Biol.* **344** 135

[23] Yang M 2006 *J. Mol. Spectrosc.* **239** 108

[24] Kolli A, O'Reilly E J, Scholes G D and Olaya-Castro A 2012 *J. Chem. Phys.* **137** 174109

[25] Davydov A S 1973 *J. Theor. Biol.* **38** 559

[26] Guerreschi G G, Cai J M, Popescu S and Briegel H J 2012 *New J. Phys.* **14** 053043

[27] Irish E K, G'omezbombarelli R and Lovett B W 2014 *Phys. Rev. A* **90** 012510

[28] Song W, Huang Y S and Cao Z L 2015 *Chin. Phys. Lett.* **32** 088701

[29] Chen H, Wang X, Fang A P and Li H R 2016 *Chin. Phys. B* **25** 98201

[30] Ritschel G, Roden J, Strunz W T and Eisfeld A 2011 *New J. Phys.* **13** 113034

[31] Turner D B, Dinshaw R, Lee K K, Belsley M S, Wilk K E, Curmi P M G and Scholes G D 2012 *Phys. Chem. Chem. Phys.* **14** 4857

[32] Hay S and Scrutton N S 2012 *Nat. Chem.* **4** 161

[33] Wilk K E, Harrop S J, Jankova L, Edler D, Keenan G, Sharples F, Hiller R G and Curmi P M 1999 *Proc. Natl. Acad. Sci. USA* **96** 8901

[34] Olaya-Castro A, Lee C F, Olsen F F and Johnson N F 2007 *Phys. Rev. B* **78** 085115

[35] Chin A W, Prior J, Rosenbach R, Caycedo-Soler F, Huelga S F and Plenio M B 2013 *Nat. Phys.* **9** 113

[36] Huelga S F and Plenio M B 2014 *Nat. Phys.* **10** 621

[37] Yang S, Xu D Z, Song Z and Sun C P 2010 *J. Chem. Phys.* **132** 234501

[38] Panitchayangkoon G, Hayes D, Fransted K A, Caram J R, Harel E and Wen J 2010 *Proc. Natl. Acad. Sci. USA* **107** 12766

[39] Scully M O and Zubairy M S, 1997 *Quantum Optics* (Cambridge: Cambridge University Press) p. 199

[40] Aspelmeyer M, Kippenberg T J and Marquardt F 2014 *Rev. Mod. Phys.* **86** 1391

[41] Engel G S, Calhoun T R, Read E L and Ahn T 2007 *Nature* **446** 782

[42] James D F V 2000 *Fortschritte Der Physik* **48** 823